



Organ Size Control via Hydraulically Gated Oscillations

Citation

Ruiz-Herrero, Teresa, Kévin Alessandri, Basile V. Gurchenkov, Pierre Nassoy, and L. Mahadevan. 2017. Organ Size Control via Hydraulically Gated Oscillations. *Development* 144: 4422-4427.

Published version

<https://doi.org/10.1242/dev.153056>

Link

<http://nrs.harvard.edu/urn-3:HUL.InstRepos:40986244>

Terms of use

This article was downloaded from Harvard University's DASH repository, and is made available under the terms and conditions applicable to Other Posted Material (LAA), as set forth at

<https://harvardwiki.atlassian.net/wiki/external/NGY5NDE4ZjgzNTc5NDQzMGIzZWZhMGFIOWI2M2EwYTg>

Accessibility

<https://accessibility.huit.harvard.edu/digital-accessibility-policy>

Share Your Story

The Harvard community has made this article openly available.

Please share how this access benefits you. [Submit a story](#)

RESEARCH ARTICLE

Organ size control via hydraulically gated oscillations

Teresa Ruiz-Herrero¹, Kévin Alessandri^{2,3}, Basile V. Gurchenkov^{4,5,6,7}, Pierre Nassoy^{2,3} and L. Mahadevan^{1,8,*}

ABSTRACT

Hollow vesicular tissues of various sizes and shapes arise in biological organs such as ears, guts, hearts, brains and even entire organisms. Regulating their size and shape is crucial for their function. Although chemical signaling has been thought to play a role in the regulation of cellular processes that feed into larger scales, it is increasingly recognized that mechanical forces are involved in the modulation of size and shape at larger length scales. Motivated by a variety of examples of tissue cyst formation and size control that show simultaneous growth and size oscillations, we create a minimal theoretical framework for the growth and dynamics of a soft, fluid-permeable, spherical shell. We show that these shells can relieve internal pressure by bursting intermittently, shrinking and re-growing, providing a simple mechanism by which hydraulically gated oscillations can regulate size. To test our theory, we develop an *in vitro* experimental set-up to monitor the growth and oscillations of a hollow tissue spheroid growing freely or when confined. A simple generalization of our theory to account for irreversible deformations allows us to explain the time scales and the amplitudes of oscillations in terms of the geometry and mechanical properties of the tissue shells. Taken together, our theory and experimental observations show how soft hydraulics can regulate the size of growing tissue shells.

KEY WORDS: Morphogenesis, Hydraulic gating, Organ size control, Synthetic cysts

INTRODUCTION

Biological organs are formed via iterations and variations of just a few geometric/topological themes: folding, lumenization and segmentation. The regulation of their size and shape is crucial for normal physiological function in organisms (Conlon and Raff, 1999; Day and Lawrence, 2000; Serrano and O'Farrell, 1997). In addition to molecular and cellular chemical patterning, it is becoming increasingly clear that mechanical forces play an important role in regulating the size and shape of tissues, organs and organisms. These forces arise from differential growth or movement, confinement, and active processes such as contraction, division and apoptosis. Given the large water content in tissues, it is

also likely that hydraulics plays an important role in creating and regulating size and shape at multiple levels. Indeed, at the cellular level, the role of water movements has led to a re-evaluation of cytoplasmic mechanics (Moeendarbary et al., 2013). At the organ level, we know that cysts and tubules (O'Brien et al., 2002) enclosing a central lumen are a common motif in the brain, the gut tube, the otic vesicle, kidneys, etc. (Desmond and Jacobson, 1977; Tanner et al., 1995). Fluid pressure is thought to play an important role in the early growth and shaping of vesicular structures that grow by inflation, and for an organ to become functional tissue growth and cyst growth need to be coordinated; failure to achieve this results in many diseases (Desmond and Jacobson, 1977; Navis and Bagnat, 2015; Tanner et al., 1995).

As natural occurrences of this, we note that the formation and hatching of blastocysts in amniote embryos (Biggers et al., 1988; Watson, 1992), regeneration in primitive Cnidarians such as *Hydra vulgaris* (Fütterer et al., 2003), and inner ear morphogenesis and stability are all dependent on tissue hydraulics (Hoijsman et al., 2015). In each case, lumenization proceeds via inhomogeneous fluid pumping into an otherwise homogeneous cellular aggregate, which nucleates a cavity that then grows. In all cases, the inflated hollow cellular shell undergoes periodic oscillations in size even as it maintains an average radius stably over hours and even days (Fig. 1). For example, the blastocyst, formed after cavitation of the mammalian zygote, consists of a shell composed of two layers, the zona pellucida and the trophectoderm, that surround an internal cavity filled with fluid (Biggers et al., 1988; Watson, 1992). The blastocyst increases its total average volume via a series of slow expansions and rapid contractions during which fluid is pumped in and out (Cole, 1967; Niimura, 2003), eventually reaching a critical size before it hatches by creating a small tear in the zona pellucida that grows and allows the whole blastocyst to escape. The contractions and expansions are thought to play an active role in thinning out and softening the outer layer (Cole, 1967; Niimura, 2003). In the context of the inner ear, studies in the zebrafish suggest that hydrostatic pressure of the endolymph fluid drives early ear growth, and subsequent volume homeostasis is needed for proper function (Hoijsman et al., 2015). Finally, at the level of an entire organism, young specimens of the Cnidarian *H. vulgaris* consist of a hollow sphere of cells that undergoes cycles of contractions and expansions driven by the hydrostatic pressure that builds up and leads to tissue bursting, causing a sudden increase of permeability (Fütterer et al., 2003; Kücken et al., 2008), followed by healing before the cycle is repeated. After several oscillations, spherical symmetry is broken causing elongation along an axis (Soriano et al., 2006). Inflation-deflation oscillations are also observed after cavitation in organoids cultured *in vitro* [see supplementary movies in Drost et al. (2015), Farin et al. (2016), Jaffe et al. (2008), Sato et al. (2009)], although these oscillations have not been explicitly studied in that context.

In each of these systems, which span different organs and organisms, we see that a spherical hollow tissue grows via fluid permeation and cellular division, distending until it bursts, before the cycle is repeated. This suggests that there is likely to be a

¹Paulson School of Engineering and Applied Sciences, Harvard University, Cambridge, MA 02138, USA. ²Université de Bordeaux, Talence 33405, France.

³Institut d'Optique Graduate School & CNRS, LP2N, Talence F-33405, France.

⁴Institut de Génétique et de Biologie Moléculaire et Cellulaire, 67404 Illkirch-Graffenstaden, France. ⁵Centre National de la Recherche Scientifique, UMR7104, 67404 Illkirch-Graffenstaden, France. ⁶Institut National de la Santé et de la Recherche Médicale, U964, 67404 Illkirch-Graffenstaden, France. ⁷Université de Strasbourg, 67404 Illkirch-Graffenstaden, France. ⁸Departments of Physics and Organismic and Evolutionary Biology, Wyss Institute for Biologically Inspired Engineering and Kavli Institute for NanoBio Science and Technology, Harvard University, Cambridge, MA 02138, USA.

*Author for correspondence (lmahadev@g.harvard.edu)

 L.M., 0000-0002-5114-0519

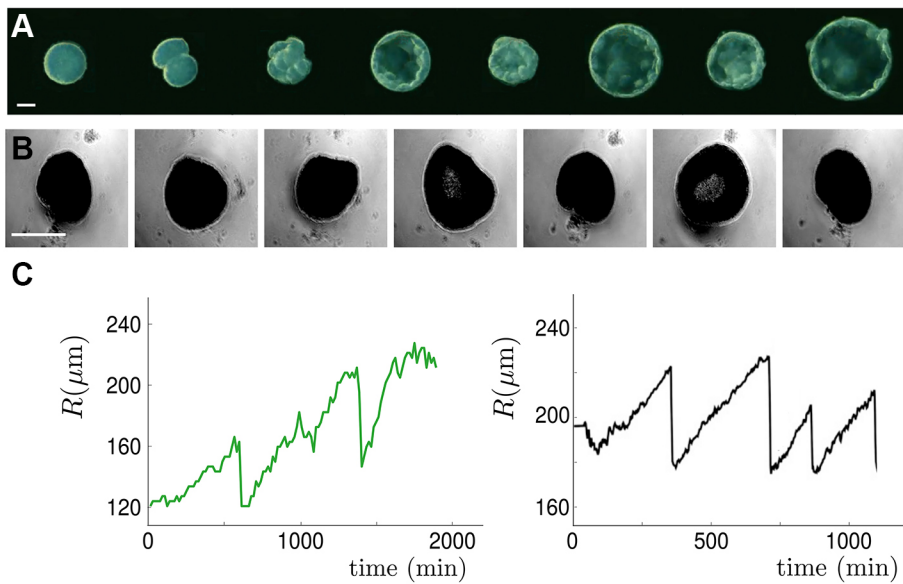


Fig. 1. Oscillations of a spherical multicellular tissue vesicle. (A) Blastocyst formation in a developing human embryo, showing the first cell divisions and the formation of the blastocyst cavity (figure adapted from Wong et al. 2010). (B) Swelling-collapse oscillations during *H. vulgaris* regeneration (figure adapted from Soriano et al., 2006). (C) Time evolution of the radius for the two cases: blastocyst (green) and *Hydra* (black). The blastocyst trajectories were obtained from the analysis of the movies in the supplementary information of Wong et al. (2010), and the *Hydra* trajectory from Soriano et al. (2006). Scale bars: 100 μm (A); 200 μm (B).

common physical scenario to explain this dynamic process. Here, we provide a mathematical model that shows how hydraulically gated oscillations can provide a robust and efficient way of controlling the size of multicellular tissue cysts. To test our predictions, we introduce an *in vitro* experimental system for the study of oscillations in synthetic cysts and show how our general theory is consistent with our experimental observations.

RESULTS

Theory

To describe the growth and dynamics of a cyst, a multicellular cyst, we assume it has the shape of a simple spherical shell filled with fluid at a different pressure relative to the environment, as shown in Fig. 2A. Cell proliferation changes the volume of the wall occupied by cells, and any osmotic imbalance or active pumping creates an inward flux of solvent that increases the radius of the shell while stressing its wall. When the wall stress is greater than a critical

threshold, the wall ruptures leading to an outward flux that reduces the wall tension and deflates the shell. This deflation allows the rupture to heal, and the whole process repeats itself. To understand this quantitatively, we start with a minimal model that assumes that cell proliferation and osmotic influx rate ($J_o = KP_{osm}$) are constant and independent of the tension, and that the material is purely elastic. Then, we may write a set of equations for the evolution of the radius of the shell $R(t)$, the thickness $h(t)$, the hydrostatic pressure $P(t)$ and the wall stress $\sigma(t)$ that couples cell proliferation, and fluid permeation to the generation of tension in the tissue wall, and its intermittent release, and reads as:

$$4\pi \frac{d}{dt} (R^2 h) = J_c \quad (\text{cell volume conservation}), \quad (1)$$

$$\frac{dR}{dt} = K(P_{osm} - P) - Q \quad (\text{lumen volume conservation}), \quad (2)$$

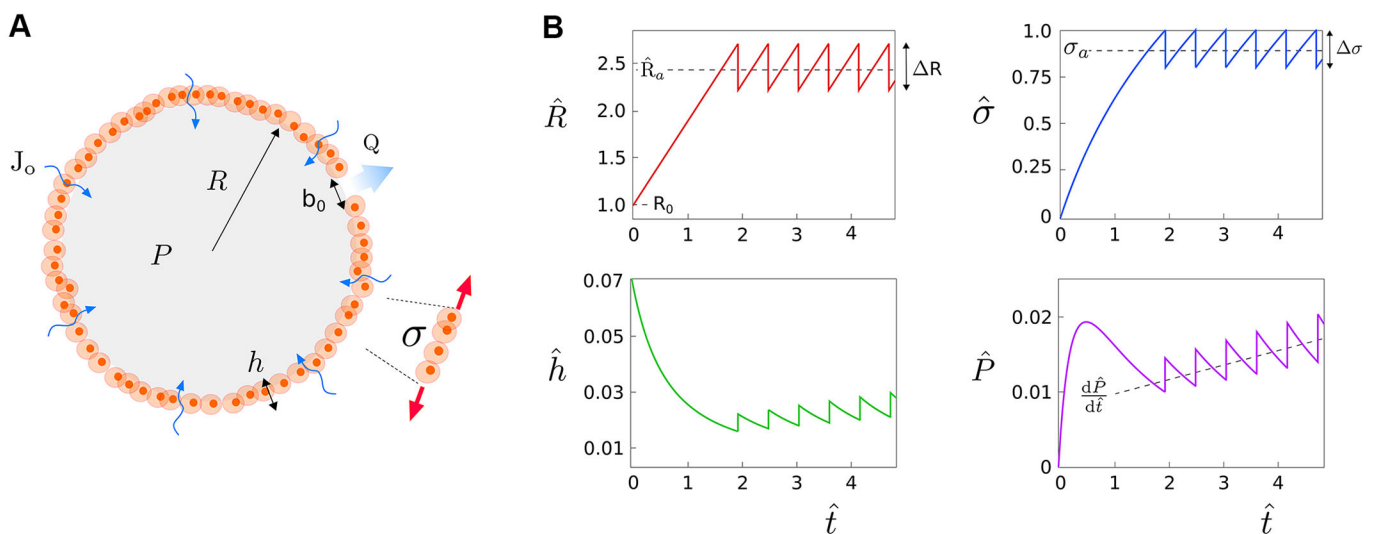


Fig. 2. Mathematical model of oscillations in the size of a spherical shell. (A) System schematic depicting the main quantities: cyst radius (R) and thickness (h), hydrostatic pressure (P), surface tension (σ), constant inward flux due to osmotic pressure (J_o) and outward flux (Q) that releases the pressure when a hole of size b_0 opens. (B) Oscillatory dynamics for the scaled radius, surface tension, thickness and pressure obtained from solving numerically the system of differential Eqns 6-8 with the following parameter values $\hat{j} = 0.016$, $e = 9.28 \cdot 10^{13}$, $\hat{\sigma}_2 = 1$, $\hat{h}_0 = 0.07$, $\hat{b}_0 = 0.036$, $\Delta \hat{\sigma} = 0.2$, $\hat{\sigma}_0 = \hat{P}_0 = 0$.

$$\sigma = \frac{PR}{2h} \quad (\text{tangential force balance on shell}), \quad (3)$$

$$\frac{d\sigma}{dt} = \frac{E}{R} \frac{dR}{dt} \quad (\text{elastic constitutive equation}), \quad (4)$$

where J_c is the cell proliferation rate, K the areal permeability of the tissue wall, P_{osm} the osmotic pressure, Q the water efflux rate after rupture per unit area of the shell, and E the elastic modulus of the tissue. We further assume that when the wall ruptures, outward flow through the resulting hole can be modeled via a simple linear Poiseuille-like relation coupling pressure to flux that reads:

$$Q = \frac{1}{4\pi R^2} \frac{r^4 P}{\eta h}, \quad (5)$$

where η is the viscosity of the solvent and r is the radius of the hole. We further assume that the time scale for hole closing is much shorter than the time scale for tissue growth, i.e. $\tau_{\text{hole}} \ll \tau_{\text{growth}}$, so that we can approximate the opening of the hole as a sigmoid that depends on the wall stress. Then the hole has only two possible states, open and closed, and the transition between them occurs when the tension reaches the rupture tension, i.e. $\sigma = \sigma_2$, leading to a hole of radius r_b that closes when the fluid flow through the hole causes the tension to decrease to the healing tension, i.e. $\sigma = \sigma_1$ (Fig. S3) (see supplementary information where we relax these assumptions and discuss their effects, Fig. S6). This model bears some resemblance to the one proposed for *H. vulgaris* regeneration (Fütterer et al., 2003; Kücken et al., 2008). However, our model accounts for tissue growth and tension-controlled rupture and healing; in the following sections, we will also introduce noise, multiple layers and different mechanical dependencies.

Analysis

To understand the dependence of the system on the different parameters, we can rewrite Eqns 1-5 in their dimensionless form scaling the length by the initial radius R_0 , time by the time scale of cyst expansion $\tau_{\text{growth}} = R_0/J_c$ and tension and pressure by the elastic modulus E , writing: $\hat{R} = R/R_0$, $\hat{h} = h/R_0$, $\hat{\sigma} = \sigma/E$, $\hat{P} = P/E$, $\hat{t} = t/\tau_{\text{growth}}$. Simplifying the dimensionless system of equations, we can follow the evolution of the scaled radius, thickness and lumen pressure via the system:

$$\frac{d\hat{R}}{d\hat{t}} = (1 - \hat{P}/\hat{P}_{\text{osm}} - \hat{Q}) \equiv \hat{\Phi}, \quad (6)$$

$$\frac{d\hat{h}}{d\hat{t}} = \hat{j} \frac{1}{\hat{R}^2} - \frac{2\hat{h}}{\hat{R}} \hat{\Phi}, \quad (7)$$

$$\frac{d\hat{P}}{d\hat{t}} = \frac{1}{\hat{R}^2} \left((2\hat{h} - 3\hat{P}\hat{R}) \hat{\Phi} + \hat{j} \frac{\hat{P}}{\hat{h}} \right), \quad (8)$$

where $\hat{\Phi} = \Phi/J_c$ is the dimensionless net flux, $\hat{j} = \frac{J_c}{4\pi R_0^2 J_0}$ is the dimensionless ratio between the proliferation rate and the influx rate, and \hat{Q} is a function of the dimensionless variables that reads

$$\hat{Q} = e \frac{\hat{r}^4 \hat{P}}{\hat{R}^2 \hat{h}} H(\sigma - \sigma_2), \quad (9)$$

with $e = ER_0/4\pi\eta J_0$. We see that the dimensionless parameters that specify the dynamics are $J_c/J_0 R_0^2$ (the change in volume in the spherical shell over the change relative to the internal cyst volume), $ER_0/\eta J_0$ (the ratio between the time scales for cyst expansion and

mechanical deformation) and $\Delta\sigma/E$ (the strain amplitude that the cyst experiences during oscillations).

This system of Eqns 6-9 has no fixed points for non-zero radius R or thickness h of the cyst; however, the presence of different thresholds for rupture and healing suggests the possibility of oscillatory dynamics. To understand this, we first provide a simple analytical approach for the period and amplitude of the ensuing oscillations. Assuming that oscillations arise in the limit of a weakly strained shell, i.e. $\epsilon \ll 1$, with the stresses lying between the two limits associated with rupture σ_2 and healing σ_1 , we write $\Delta\hat{\sigma} = (\sigma_2 - \sigma_1)/E$, neglecting for simplicity the contribution of the hydrostatic pressure to the flux, assuming it is small for soft elastic materials, i.e. $P/P_{\text{osm}} \ll 1$. For a cyst with dimensionless average radius (\hat{R}_a) and amplitude of oscillations ($\Delta\hat{R}$), the strain is approximately $\Delta\hat{R}/\hat{R}_a$ and:

$$\Delta\hat{\sigma} = \frac{\Delta\hat{R}}{\hat{R}_a}. \quad (10)$$

Assuming that we start with an initial cyst that is tensionless, the change in radius from the initial value R_0 to the average value R_a follows:

$$\frac{R_a - R_0}{R_0} \sim \sigma_2/E. \quad (11)$$

Then Eqns 10 and 11 imply that the average scaled radius and the scaled amplitude for oscillations are given by:

$$\hat{R}_a \sim (1 + \hat{\sigma}_2), \quad (12)$$

$$\Delta\hat{R} = \Delta\hat{\sigma}(1 + \hat{\sigma}_2), \quad (13)$$

which in dimensional form read $R_a \sim R_0(1 + \sigma_2/E)$ and $\Delta R = (R_0 \Delta\sigma/E)(1 + \sigma_2/E)$. Similarly, from Eqns 6, 8 and 12, we see that the average thickness and pressure increase for $\hat{J}_c \neq 0$ follow the relations:

$$\frac{d\hat{h}_a}{d\hat{t}} \sim \frac{\hat{J}_c}{(1 + \hat{\sigma}_2)^2}, \quad (14)$$

$$\frac{d\hat{P}_a}{d\hat{t}} \sim \frac{2\hat{\sigma}_a d\hat{h}_a}{\hat{R}_a d\hat{t}} = \hat{J}_c \frac{2\hat{\sigma}_2 - \Delta\hat{\sigma}}{(1 + \hat{\sigma}_2)^3}, \quad (15)$$

with $\hat{J}_c = J_c \tau_{\text{growth}}/4\pi R_0^3$. Finally, the period of the oscillations, τ_{osc} , is set by the time needed to increase the cyst volume from the minimum size $R_{\text{min}} = R_a - \Delta R/2$ to the maximum size $R_{\text{max}} = R_a + \Delta R/2$:

$$\hat{\tau}_{\text{osc}} = \frac{\tau_{\text{osc}}}{\tau_{\text{growth}}} = \Delta\hat{R} = \Delta\hat{\sigma}(1 + \hat{\sigma}_2). \quad (16)$$

To test the validity of our simple analysis, we solve the ordinary differential equation (ODE) system Eqns 6-8 numerically for a range of parameters consistent with experiments that correspond to $\hat{j} = 0.016$, $e = 9.28 \cdot 10^{12}$, $\hat{\sigma}_2 = 1$, $\hat{h}_0 = 0.07$, $\Delta\hat{\sigma} = 0.2$, $\hat{\sigma}_0 = \hat{P}_0 = 0$. In Fig. 2B, we show a set of trajectories for the variations of R , h , σ and P ; as expected, the cyst grows from an initial state and then starts to oscillate asymmetrically because the time scale for rupture is much faster than that of growth. Consistent with our scaling predictions (Fig. S4), we see that both the radius and the tension oscillate with period τ_{osc} around a constant value after an initial increase. We also see that the cyst thickness and pressure can increase or decrease during the first stage before oscillations appear, depending on the ratio $J_c/J_0 R_0^2$ and the initial values h_0 , R_0 and P_0 (see Eqn 7). If the initial tension and pressure are different from zero, this will affect the initial growth phase, and yield a different value for the maximum size, but all our qualitative

results will remain similar. When the cells in the shell proliferate $J_c \neq 0$; the average values of the pressure and thickness, as well as the amplitude of their oscillations increase linearly, consistent with our analytical estimates (Eqns 14, 15).

Experiments

To test these theoretical ideas in an experimental setting, we developed an artificial set-up using multicellular cysts for which oscillations and growth can be easily monitored. Cysts were prepared from MCF10-DCIS.com cells using the Cellular Capsules Technology as described by Alessandri et al. (2013) for multicellular spheroids (see schematics in Fig. 3A). Briefly, a composite fluid jet is generated using a co-extrusion method with cells in suspension in the core flow and a polysaccharide (alginate) that undergoes gelation in contact with divalent ions in the sheath flow. Following encapsulation, we observe that cells which are confined in the aqueous core of the hollow permeable capsule divide and occupy an increasing volume of the capsule. Confocal micrographs of the equatorial plane of the encapsulated multicellular aggregates show that the spheroids are hollow (Fig. S1). Confocal live imaging of the cyst surface also reveals a honeycomb-like structure, which is typical of epithelia (Movie 1).

We further monitored the growth dynamics of individual cysts by phase contrast microscopy by acquiring time-lapse sequences over extended periods of times (~ 15 days). Fig. 1C and Movies 2-4 show typical sequences of cyst oscillations. We immediately remark that cyst average radii increase in time from one cycle to another with several different scenarios seen: (1) when $R_{\text{cyst}} < R_{\text{capsule}}$, the cyst expands and shrinks freely (Movie 2); (2) when $R_{\text{cyst}} > R_{\text{capsule}}$, the cyst expands against an elastic micro-compartment (Movie 3); (3) for large deformations of the capsules, the capsule occasionally bursts out and the cyst may escape (a phenomenon that is strongly reminiscent of blastocyst hatching in embryos), before resuming free oscillations (Movie 4). We also observe that the oscillation amplitude and period are altered once the cyst reaches the wall of the capsule. More quantitatively, representative temporal evolutions of cyst radius are shown in Fig. 3B (central panel) and Fig. S2.

Complementary experiments were performed to measure the characteristic time for hole closing, τ_{hole} . We were able to capture deflation events by chance (Movie 5). In parallel, we also carried out punching experiments with a micro-manipulator glass needles of typical diameter $\sim 10 \mu\text{m}$ (Movie 6). In both cases, deflation dynamics (Fig. S2) show that τ_{hole} is ~ 1 -2 min. As hypothesized in the rest of the manuscript, $\tau_{\text{growth}} \gg \tau_{\text{hole}}$. All together, we see that whereas the free cyst oscillates in size with increasing average radius, after confluence the cyst is confined by the capsule and both of them oscillate jointly with a period longer than that observed during the free stage.

A qualitative test of our theory requires perturbation experiments to modulate the dynamics of cyst oscillations. This can be achieved either by molecular control of the permeation dynamics or by varying the external osmolarity. The former is not likely to shed any light on the general mechanisms as it would target specific membrane channels and cannot rule out the role of other compensatory mechanisms. Therefore, we performed the qualitative experiment of increasing the environmental osmolarity, and see that the elimination of an osmotic pressure difference completely inhibits cyst oscillations, consistent with our simple theory.

Adapting the model to experiments

Our simple elastic model for the dynamics of cysts predicts size oscillations between a maximum and a minimum radius associated with hole opening and healing (Fig. 2B). However, it fails to explain the steady increase in the average radius and the effect of confinement observed in our experiments, most likely because the assumption of a purely elastic response is less realistic than a viscous or plastic rheology for the multicellular tissue. Therefore, we modify our choice of a simple linear elastic-plastic material law for tissue behavior (see supplementary information for details, and also for a comparison with the use of a viscous law, see Fig. S7). A linear elastic-plastic response ensures stress relaxation after deformations, allowing us to represent implicitly cell rearrangements driven by cell migration, division and death. Below the yield stress, σ_y , the strain-stress relation is assumed to be elastic with a modulus E , whereas above it we assume that the modulus is $H < E$, so that after

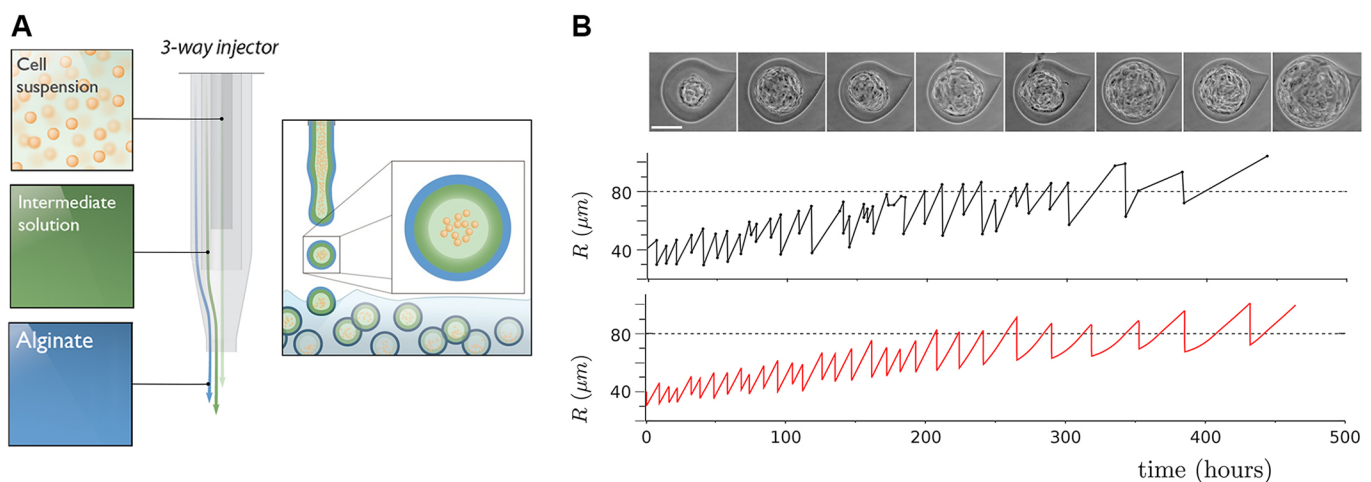


Fig. 3. Experiments to create and study synthetic multicellular tissue shells. (A) Experimental set-up formed by a microfluidic co-extrusion device. The spheroids were formed by an outer sheath of a sodium alginate solution and an inner core composed of a cell suspension. (B) Top: Snapshots showing cysts of MCF-DCIS.com cells inside alginate capsules that undergo cycles of expansion and shrinkage. Scale bar: 100 μm . Bottom: Comparison between experimental observations (black) and theoretical results (red) for the evolution of the cyst radius. The dashed line shows the initial radius of the alginate capsule. The numerical results were obtained using the following parameters and initial conditions: $J_c = 2 \mu\text{m h}^{-1}$, $J_e = 8 \mu\text{m}^3 \text{h}^{-1}$, $E_c = 20 \text{ kPa}$, $H_c = 16 \text{ kPa}$, $E_a = 70 \text{ kPa}$, $\bar{\sigma}_2 = 11 \text{ kPa}$, $\bar{\sigma}_1 = 4.4 \text{ kPa}$, $\sigma_y = 8.5 \text{ kPa}$, $R_c(0) = 40 \mu\text{m}$, $R_a(0) = 80 \mu\text{m}$, $h_c(0) = 6 \mu\text{m}$, $h_a(0) = 20 \mu\text{m}$, $b_0 = 5 \mu\text{m}$, where subscript c stands for cyst and a for alginate capsule.

the first oscillation $\epsilon_1 = \sigma_y/E + (\sigma_2 - \sigma_y)/H$. In the first phase, when the cyst grows unimpeded, $\sigma_y \leq \sigma_2$ and plastic deformations will occur during every oscillation and the average radius will increase accordingly (Fig. S5; Fig. 3B). Then after the i th oscillation, the strain and radius evolves as follows:

$$\epsilon = \epsilon_i - \frac{\sigma_2 - \sigma_y}{E} + \frac{\sigma - \sigma_y}{H}, \quad (17)$$

$$\epsilon_i = \epsilon_1 + i\Delta\epsilon, \quad (18)$$

$$R_i = R_1(1 + \Delta\epsilon)^{i-1}, \quad (19)$$

with R_1 being the maximum radius and ϵ_1 the maximum strain before the first deflation and $\Delta\epsilon = (\sigma_2 - \sigma_y)(1/H - 1/E)$.

In the second phase, cyst growth is slowed down owing to confinement by the alginate elastic capsule. The presence of a second stiff layer implies that part of the tangential stress in the pressurized tissue is taken up by the alginate shell, so that a higher inner pressure is necessary for continued growth. As observed in Eqn 6, this increase in the hydrostatic pressure is translated into a decrease in the net flux and therefore a smaller period of oscillations (Eqn 16; Fig. 3B). To obtain the evolution of the cyst radius, thickness, pressure and period of oscillations, we use the ODE system Eqns 6-8, leaving them in dimensional form for ease of comparison with experiments, but modifying Eqn 8 to account for the variation in the total tension to read:

$$\frac{P\bar{R}}{2h_{\text{tot}}} = \sigma_c + \sigma_a, \quad (20)$$

where subscript c stands for cyst and a for alginate capsule, and $\bar{R} = (R_c + R_a)/2$, $h_{\text{tot}} = h_c + h_a$. Because both layers are in contact, they undergo the same displacement. Assuming small variations in the thickness, and further that the thickness is much smaller than the radius, this implies that $dR_c/dt = dR_a/dt$. Using these approximations, we obtain a variant of the system of differential equations (Eqns 6-8) to describe the experimental system:

$$\frac{dR_c}{dt} = \frac{dR_a}{dt} = K(P_{\text{osm}} - P) - Q \equiv \Phi, \quad (21)$$

$$\frac{dh_c}{dt} = \frac{J_c}{4\pi R_c^2} - 2\frac{h_c}{R_c}\Phi, \quad \frac{dh_a}{dt} = -2\frac{h_a}{R_a}\Phi, \quad (22)$$

$$\frac{d\sigma_c}{dt} = \frac{E_c}{R_c}\Phi, \quad \frac{d\sigma_a}{dt} = \frac{E_a}{R_a}\Phi, \quad (23)$$

with the hydrostatic pressure following:

$$\frac{dP}{dt} = \frac{2\Phi}{\bar{R}} \left[h_{\text{tot}} \left(\frac{E_c}{R_c} + \frac{E_a}{R_a} \right) - \frac{P}{2} + \frac{P\bar{R}}{h_{\text{tot}}} \left(\frac{J_c}{8\pi\Phi R_c^2} - \frac{h_c}{R_c} - \frac{h_a}{R_a} \right) \right]. \quad (24)$$

To solve the system Eqns 21-24 and 17, we used the following parameter values measured experimentally: tissue elastic modulus $E_c = 20$ kPa, alginate elastic modulus $E_a = 70$ kPa, osmotic flux $J_o = 2 \mu\text{m h}^{-1}$, plastic modulus $H_c = 16$ kPa, tissue permeability $K = 0.1 \mu\text{m/kPa} \cdot \text{h}$, cell replication rate $J_c = 8 \mu\text{m}^3 \text{h}^{-1}$, initial radius of the cyst $R_c(0) = 40 \mu\text{m}$ and its thickness $h_c(0) = 6 \mu\text{m}$, radius of the alginate shell $R_a(0) = 80 \mu\text{m}$ and its thickness $h_a(0) = 20 \mu\text{m}$. The elastic moduli were chosen to be within the ranges measured experimentally (Alessandri et al., 2013; Harris et al., 2012), the osmotic flux, the plastic coefficient, the rupture tension and the initial state were estimated from the experimental results, and the cell replication rate corresponds approximately to the division rate of one cell per day observed in experiments. Finally, the experiments show that

oscillations are likely to be neither purely deterministic or stochastic, but a mixture of the two. The cyst dynamics is affected by noise because rupture is a catastrophic event that depends on material inhomogeneities. Introducing noise by allowing the rupture and healing tensions to fluctuate randomly around their average values following a Gaussian distribution with $\sigma_i \in \mathcal{N}(\bar{\sigma}_i, 0.4)$, we obtained trajectories that fit the experimental results (Fig. 3B). This agreement shows that a simple but natural extension of our general model to account for plasticity of the tissue, and the elastic confinement by an alginate shell suffices to explain our experimental observations.

DISCUSSION

Size control requires the use of dynamic measurements to measure and control shape. As examples at the molecular scale, we point to microtubule length oscillations in asters, and at the cellular scale, we point to the ruffling oscillations in cells that are used to measure confluence. Here, we have presented a simple but general framework for tissue size control, inspired by the relatively common example of fluid-driven growth and hydraulically gated oscillations seen in diverse multicellular hollow tissue vesicles such as organoids, blastocysts, zebrafish inner ear and even body regeneration in *H. vulgaris*.

A crucial fact that underlies our study is that there is a large separation of time scales associated with the relatively fast rupture and leakage of luminal fluid when the tissue stress reached a critical value, and the slow growth of the lumen via permeation. This allows for robust regulation of cyst size via hydraulically gated oscillations. We present an analytical theory for the case of small strains in an elastic shell that yields simple expressions for the average size of the vesicle, and the frequency and amplitude of size oscillations, and complements a more general framework that accounts explicitly for complex mechanical properties and different functional forms for transport and growth. We also performed experiments in a synthetic set-up that showed the predicted oscillatory behavior, but to explain the gradual increase in the radius and the period of oscillation, we generalized our theory to include an elastic-plastic response for the tissue to describe the large strain behavior observed in our experiments.

The abrupt increase of the permeability of the cyst in our simple setting was associated with the formation of a simple hole. However, the pressure relief mechanism can take a variety of forms: localized channels, homogenous pores throughout the tissue or valves. Our coarse-grained model does not distinguish between these different mechanisms as long as the dynamics of opening and closure are faster than the cyst expansion and cell division rates, allowing us to model the outflow by an effective fast flux without focusing on the specifics. Natural extensions of this model include considerations of inhomogeneous spatial mechanical properties, active control of pressure relief via stretch-dependent valves, channels etc. and would allow us to understand how vesicular organs of a given size might be shaped by fluid pressure.

MATERIALS AND METHODS

Cell culture

We used wild-type MCF10DCIS.com cells (Asterand) and MCF10DCIS.com cells stably transfected with LifeAct-mCherry. Cells were maintained in DMEM-F12 (50:50) supplemented with 5% horse serum, 2 mM L-glutamine, and penicillin/streptomycin in a humidified atmosphere containing 5% CO₂ at 37°C, with medium changed every 2 days. Culture media were purchased from Invitrogen and antibiotics from Gibco BRL.

Cell encapsulation

We used the Cellular Capsules Technology described by Alessandri et al. (2013). This method is based on a microfluidic co-extrusion device

(Fig. 3A). The outer sheath is made of a sodium alginate solution and the inner core is composed of the cell suspension obtained after trypsinization of DCIS cells cultured in a Petri dish. Liquid extrusion is performed in the air with flow rates in the range of 50-100 ml/h, which leads to the formation of a jet that fragments into droplets (due to Plateau-Rayleigh instability). Because alginate undergoes gelation in the presence of divalent ions, composite droplets readily crosslink as shells encapsulating cells upon contact with a calcium bath. The intermediate capillary is filled with a calcium-free solution (e.g. sorbitol) that serves as a barrier to diffusion of calcium released from intracellular stores, and thus avoids blockage of the chip. Once cellular capsules were formed, they were transferred within 2 min into culture medium and placed inside an incubator (37°C, 5% CO₂, ~100% relative humidity). In each encapsulation run, several tens of capsules were selected for monitoring cyst morphology and growth using high-resolution imaging. A key property of the alginate hydrogel is its permeability (pore size of 10-15 nm), which allows free flow of oxygen and nutrients into the capsule and permits cell proliferation. In this jetting regime, the radius of the capsules is determined by the size of the injector nozzle, and the aspect ratio h/R (shell thickness/shell radius) is set by the ratio between outer and inner flow rates. In most experiments performed and analyzed in the present work, capsule radii were ~100 µm and shell thicknesses were ~20 µm. These morphological parameters were measured precisely by phase contrast microscopy for each individual capsule that was monitored for this work. As reported by Alessandri et al. (2013), the Young's modulus of alginate gels prepared in a 100 mM calcium bath and kept in culture medium for several days is $E \sim 70$ kPa.

Immunofluorescence, live imaging and image analysis

To characterize the structure of the growing cellular aggregates, the encapsulated cell cultures were incubated with 0.5 µg/ml fluorescent phalloidin (Molecular Probes) in PBS with 1% vol/vol Triton X-100 (Sigma) at 4°C from 2 h to overnight. Actin staining was complemented with labeling of apoptosis using fluorescent antibodies against Caspase 3 (Merck, AB3623) at 1 µg/ml. By confocal microscopy (LSM710; Carl Zeiss), we checked that the growing multicellular aggregates were hollow spheroids, i.e. cysts (Fig. S1). To monitor the growth dynamics of cysts, we mostly used phase contrast microscopy. Time-lapse sequences over extended periods of times (~ 15 d) were acquired using an inverted microscope (Nikon Eclipse Ti, 10×/0.3 N.A. dry objective; Nikon Instruments) equipped with a motorized stage (Märzhäuser) and climate control system (The Brick; Life Imaging Systems). The microscope and camera (CoolSNAP HQ2; Photometrics) were driven by Metamorph software (Molecular Devices). Cyst radius measurements were obtained using ImageJ (National Institutes of Health). Live confocal imaging over shorter periods of time was also performed using an inverted (LSM710; Carl Zeiss) microscope. In this case, cysts were prepared with the MCF10DCIS.com LifeAct-mCherry stable line. Fluorescence was acquired using a 561-nm (15-mW) diode-pumped solid-state laser and a 25×/0.80 N.A. oil immersion objective.

Acknowledgements

We thank Philippe Chavier and Catalina Lodilinsky for providing MCFDCIS cells, and Albrecht Ott for the images that constitute Fig. 1B.

Competing interests

The authors declare no competing or financial interests.

Author contributions

Conceptualization: L.M., P.N.; Methodology: L.M., T.R.-H., P.N.; Software: T.R.-H.; Validation: L.M., T.R.-H., P.N.; Formal analysis: L.M., T.R.-H.; Investigation: L.M., T.R.-H., B.V.G., K.A., P.N.; Resources: P.N.; Data curation: B.V.G., K.A.; Writing - original draft: L.M., T.R.-H.; Writing - review & editing: L.M., T.R.-H., P.N.; Visualization: T.R.-H., B.V.G., K.A.; Supervision: L.M.; Project administration: L.M.; Funding acquisition: P.N.

Funding

This work was partially supported by the Agence Nationale de la Recherche (ANR) Invaders Project, and the Institut National de la Santé et de la Recherche Médicale

Programme Physicancer Inserm 2011. T.R.-H. was supported by the Fundación Ramón Areces and the Simons Foundation.

Supplementary information

Supplementary information available online at <http://dev.biologists.org/lookup/doi/10.1242/dev.153056.supplemental>

References

- Alessandri, K., Sarangi, B. R., Gurchenkov, V. V., Sinha, B., Kiessling, T. R., Fetler, L., Rico, F., Scheuring, S., Lamaze, C., Simon, A. et al. (2013). Cellular capsules as a tool for multicellular spheroid production and for investigating the mechanics of tumor progression in vitro. *Proc. Natl. Acad. Sci. USA* **110**, 14843-14848.
- Biggers, J. D., Bell, J. E. and Benos, D. J. (1988). Mammalian blastocyst: transport functions in a developing epithelium. *Am. J. Physiol.* **255**, C419-C432.
- Cole, R. J. (1967). Cinemicrographic observations on the trophoblast and zona pellucida of the mouse blastocyst. *J. Embryol. Exp. Morphol.* **17**, 481-490.
- Conlon, I. and Raff, M. (1999). Size control in animal development. *Cell* **96**, 235-244.
- Day, S. and Lawrence, P. (2000). Measuring dimensions: the regulation of size and shape. *Development* **127**, 2977-2987.
- Desmond, M. E. and Jacobson, A. G. (1977). Embryonic brain enlargement requires cerebrospinal fluid pressure. *Dev. Biol.* **57**, 188-198.
- Drost, J., van Jaarsveld, R. H., Ponsioen, B., Zimmerlin, C., van Boxtel, R., Buijs, A., Sachs, N., Overmeer, R. M., Offerhaus, G. J., Begthel, H. et al. (2015). Sequential cancer mutations in cultured human intestinal stem cells. *Nature* **521**, 43-47.
- Farin, H. F., Jordens, I., Mosa, M. H., Basak, O., Korving, J., Tauriello, D. V. F., de Punder, K., Angers, S., Peters, P. J., Maurice, M. M. et al. (2016). Visualization of a short-range Wnt gradient in the intestinal stem-cell niche. *Nature* **530**, 340-343.
- Fütterer, C., Colombo, C., Jülicher, F. and Ott, A. (2003). Morphogenetic oscillations during symmetry breaking of regenerating *Hydra vulgaris* cells. *Europhys. Lett.* **64**, 137-143.
- Gonzalez-Rodriguez, D., Guevorkian, K., Douezan, S. and Brochard-Wyart, F. (2012). Soft matter models of developing tissues and tumors. *Science* **338**, 910-917.
- Harris, A. R., Peter, L., Bellis, J., Baum, B., Kabla, A. J. and Charras, G. T. (2012). Characterizing the mechanics of cultured cell monolayers. *Proc. Natl. Acad. Sci. USA* **109**, 16449-16454.
- Hojjman, E., Rubbini, D., Colombelli, J. and Alsina, B. (2015). Mitotic cell rounding and epithelial thinning regulate lumen growth and shape. *Nat. Commun.* **6**, 7355.
- Jaffe, A. B., Kaji, N., Durgan, J. and Hall, A. (2008). Cdc42 controls spindle orientation to position the apical surface during epithelial morphogenesis. *J. Cell Biol.* **183**, 625-633.
- Kücken, M., Soriano, J., Pullarkat, P. A., Ott, A. and Nicola, E. M. (2008). An osmoregulatory basis for shape oscillations in regenerating *Hydra*. *Biophys. J.* **95**, 978-985.
- Moeendarbary, E., Valon, L., Fritzsche, M., Harris, A. R., Moulding, D. A., Thrasher, A. J., Stride, E., Mahadevan, L. and Charras, G. T. (2013). The cytoplasm of living cells behaves as a poroelastic material. *Nat. Mater.* **12**, 253-261.
- Muñoz, J. J. and Albo, S. (2013). Physiology-based model of cell viscoelasticity. *Phys. Rev. E* **88**, 012708.
- Navis, A. and Bagnat, M. (2015). Developing pressures: fluid forces driving morphogenesis. *Curr. Opin. Genet. Dev.* **32**, 24-30.
- Niimura, S. (2003). Time-lapse videomicrographic analyses of contractions in mouse blastocysts. *J. Reprod. Dev.* **49**, 413-423.
- O'Brien, L. E., Zegers, M. M. P. and Mostov, K. E. (2002). Opinion: building epithelial architecture: insights from three-dimensional culture models. *Nat. Rev. Mol. Cell Biol.* **3**, 531-537.
- Preziosi, L., Ambrosi, D. and Verdier, C. (2010). An elasto-visco-plastic model of cell aggregates. *J. Theor. Biol.* **262**, 35-47.
- Sato, T., Vries, R. G., Snippert, H. J., Van De Wetering, M., Barker, N., Stange, D. E., Van Es, J. H., Abo, A., Kujala, P. et al. (2009). Single Lgr5 stem cells build crypt-villus structures in vitro without a mesenchymal niche. *Nature* **459**, 262-265.
- Serrano, N. and O'Farrell, P. H. (1997). Limb morphogenesis: connections between patterning and growth. *Curr. Biol.* **7**, R186-R195.
- Soriano, J., Colombo, C. and Ott, A. (2006). *Hydra* molecular network reaches criticality at the symmetry-breaking axis-defining moment. *Phys. Rev. Lett.* **97**, 258102.
- Tanner, G., McQuillan, P., Maxwell, M., Keck, J. and McAteer, J. (1995). An in vitro test of the cell stretch-proliferation hypothesis of renal cyst enlargement. *J. Am. Soc. Nephrol.* **6**, 1230-1241.
- Watson, A. J. (1992). The cell biology of blastocyst development. *Mol. Reprod. Dev.* **33**, 492-504.
- Wong, C. C., Loewke, K. E., Bossert, N. L., Behr, B., De Jonge, C. J., Baer, T. M. and Reijo Pera, R. A. (2010). Non-invasive imaging of human embryos before embryonic genome activation predicts development to the blastocyst stage. *Nat. Biotechnol.* **28**, 1115-1121.

I. SUPPLEMENTARY THEORY

A. Viscoelastic case

The assumption that the tissue shell is a linearly elastic material is simple and convenient, but false. A more general constitutive law for a multi-cellular tissue cell would have to account for both its viscous and plastic behavior when deformation is followed by self-adaptation via cell rearrangement [2, 3]. In the main text we presented an elastic-plastic regime as a minimum model to reproduce the nonlinearities observed in the experiment, however, in the general case we should expect a visco-elastic or even visco-plastic regime.

Here, we briefly discuss the role of viscoelastic deformations by using

$$\dot{\sigma} + \frac{\sigma}{\tau} = \frac{E}{R} \frac{dR}{dt} \quad (\text{S1})$$

instead of the purely elastic or elastic-plastic model used in the main text. Here $\tau = \eta_{\text{cyst}}/E$, being E the elastic modulus, and η_{cyst} the viscosity of the shell. Then, the system of differential equations (6-8) in the main text are replaced by:

$$\frac{d\hat{R}}{d\hat{t}} = (1 - \hat{P}/\hat{P}_{\text{osm}} - Q/J_o) \equiv \hat{\Phi} \quad (\text{S2})$$

$$\frac{d\hat{h}}{d\hat{t}} = \frac{J_c}{4\pi R_0^2 J_o} \frac{1}{\hat{R}^2} - \frac{2\hat{h}}{\hat{R}} \hat{\Phi} \quad (\text{S3})$$

$$\frac{d\hat{P}}{d\hat{t}} = \frac{1}{\hat{R}^2} \left((2\hat{h} - 3\hat{P}\hat{R})\hat{\Phi} + \frac{J_c}{4\pi R_0^2 J_o} \frac{\hat{P}}{\hat{h}} \right) - \frac{\hat{P}R_0}{\tau J_o} \quad (\text{S4})$$

In the viscoelastic case, there is one extra dimensionless parameter accounting for the ratio between the timescales for cyst expansion and viscoelastic deformation $R_0 E / \eta_{\text{cyst}} J_o$. The additional parameter allows for the explanation of the average radius increase observed in the experiments with synthetic cysts. However, the values of the viscoelastic coefficient needed to reproduce the experimental behavior are too high to correspond to biological tissue, which has a viscosity around $10^2 \text{kPa} \cdot \text{s}$ [4] (Fig. S7)

B. Pore dynamics

The pore opening and closing can be represented in terms of a simple dynamical system :

$$\frac{dr}{dt} = a_1 r + a_2 r^3 - a_3 r^5 \quad (\text{S5})$$

$$a_1 = \frac{\sigma - \sigma_2}{4(\sigma_2 - \sigma_1)} \frac{1}{\tau_{\text{pore}}} \quad (\text{S6})$$

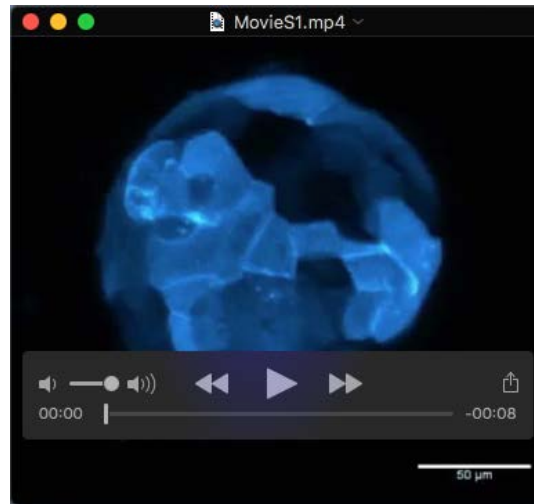
$$a_2 = \frac{1}{\tau_{\text{pore}} b_0^2} \quad (\text{S7})$$

$$a_3 = \frac{1}{\tau_{\text{pore}} b_0^4} \quad (\text{S8})$$

the normal form for a subcritical pitchfork bifurcation where the maximum pore size is b_0 and the characteristic time for healing is τ_{pore} . When the dynamics of the pore are much faster than the capsule dynamics, $\tau_{\text{pore}} \ll \tau_{\text{growth}}$, the dynamics can be approximated by a step function, in that case the pore has only two possible states and the transition between them occurs instantaneously, $r = b_0$ after it opens at $\sigma = \sigma_2$, and $r = 0$ after closing at $\sigma = \sigma_1$ (Fig.S3). If $\tau_{\text{pore}} \sim \tau_{\text{growth}}$, the pore does not heal instantaneously, and the amplitude of the oscillations varies as a function of τ_{pore} . We found that slow pore dynamics increases the amplitude and the period of oscillations while keeping the maximum radius constant (Fig.S6). This happens because although bursting occurs at the same radius for all rates of pore closing, when healing times are slower, the pore closes at smaller values of the tension, which allows more fluid to enter the cyst.

It should be pointed out that our minimal mathematical model for hole opening above a critical tissue tension has some similarities with pore opening and closing in lipid vesicles and membranes [5, 6]. However, the length and time-scales are orders of magnitude apart, and the rheology and regulatory mechanisms are very different.

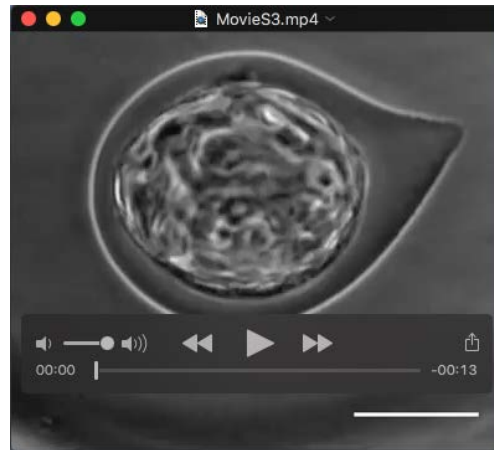
II. MOVIES



Movie 1. Confocal live imaging of an encapsulated cyst grown from cells stably transfected with LifeAct-GFP. Maximum intensity projections of the confocal stacks [a hot look-up table acquired using Fiji is shown (cyan)]. Total duration=19h



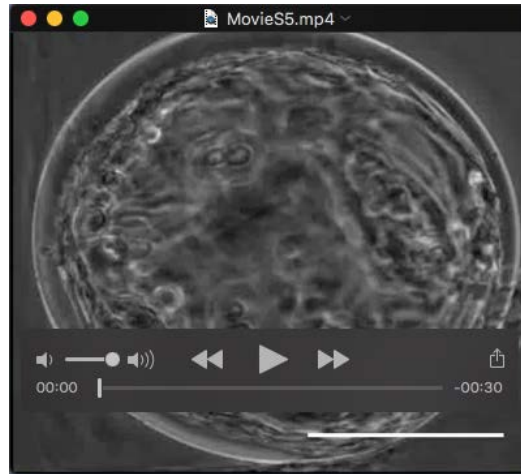
Movie 2. Growth of an MCF10DCIS.com cyst inside an alginate gel capsule. Time-lapse, phase-contrast imaging shows the oscillations of the cyst before reaching the walls of the capsule. Images were recorded every 5 min. Scale bar: 100 μm.



Movie 3. Growth of an MCF10DCIS.com cyst inside an alginate gel capsule. Time-lapse, phase-contrast imaging shows the oscillations of the cyst in contact with the capsule inner wall. Images were recorded every 5 min. Scale bar: $100\mu\text{m}$.



Movie 4. Growth of an MCF10DCIS.com cyst inside an alginate gel capsule. Time-lapse, phase-contrast imaging shows the oscillations of the cyst in contact with the capsule inner wall, bursting of the capsule, escape of the cyst, which then undergoes inflation-deflation cycles outside the capsule. Images were recorded every 5 min. Scale bar: $100\mu\text{m}$.



Movie 5. Phase contrast sequence showing the collapse of a cyst. Images were recorded every 5 s. Scale bar: $100\mu\text{m}$.



Movie 6. Phase contrast sequence of a punching experiment. An encapsulated cyst is maintained using micropipette aspiration and punched with a glass needle. Images were recorded every 1 s. Scale bar: $100\mu\text{m}$.

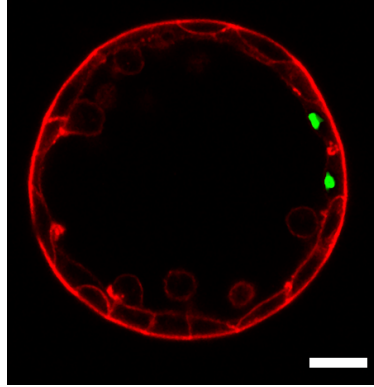


Figure S1. Confocal image of the equatorial plane of a cyst stained with for actin (red) and apoptosis (green). Scale bar: $50\mu\text{m}$.

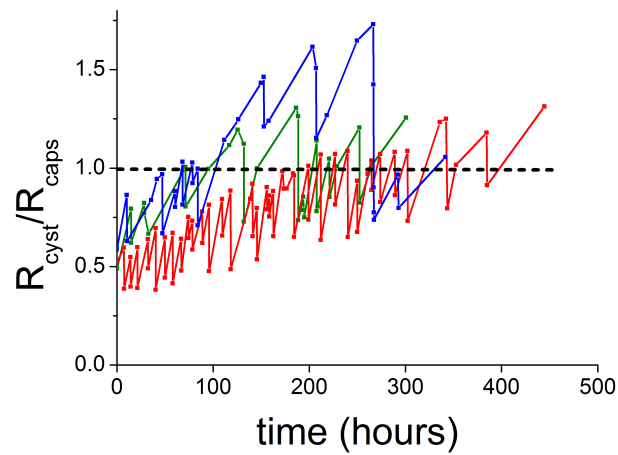


Figure S2. Representative trajectories of cyst radius for cysts with different sizes. Radius is normalized by the inner radius of the capsule.

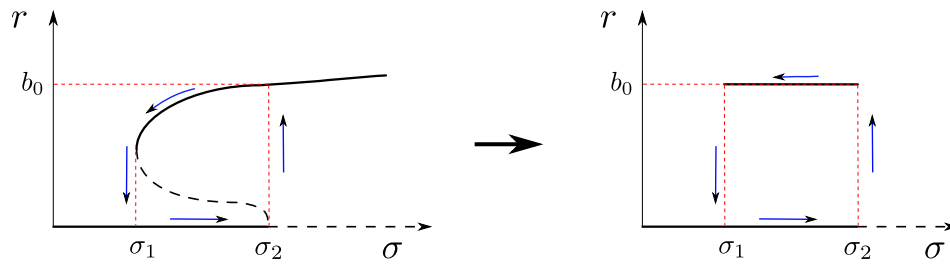


Figure S3. Subcritical pitchfork bifurcation approximated as a step function assuming that pore dynamics is much faster than growth with threshold tension for rupture (σ_2) and healing (σ_1) and pore size b_0 .

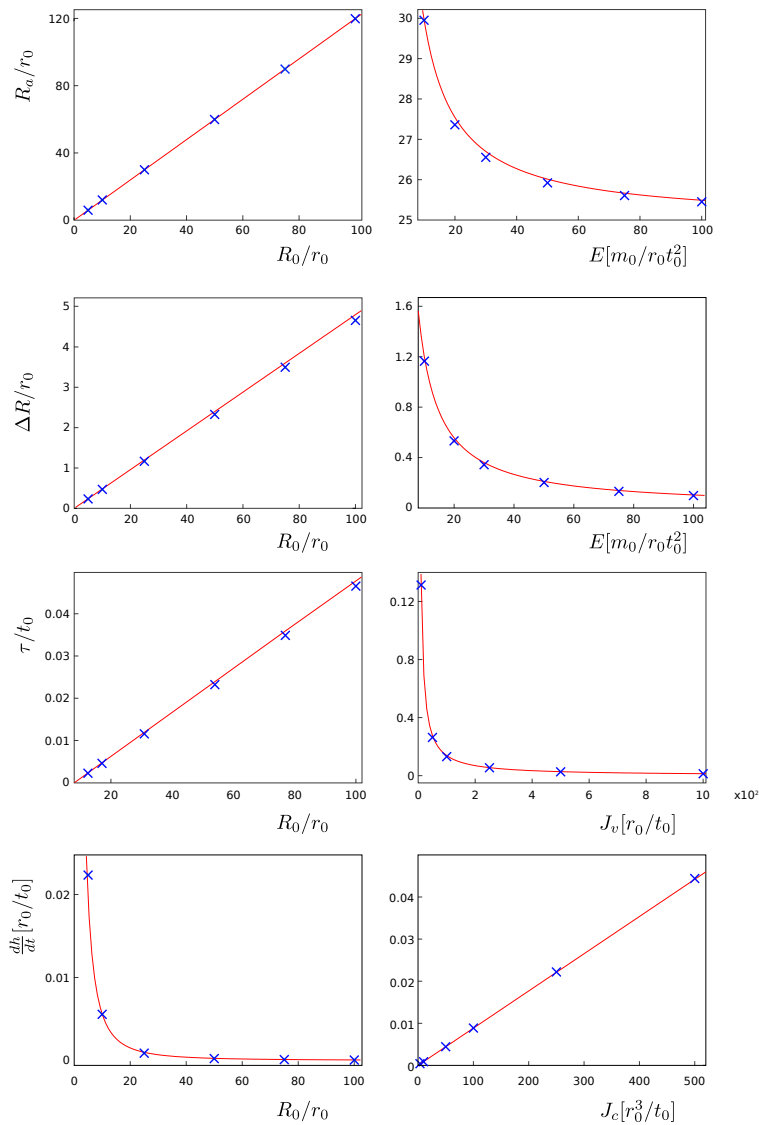


Figure S4. Comparison between theoretical estimates (line) and numerical results (cross) in the limit of small strains.

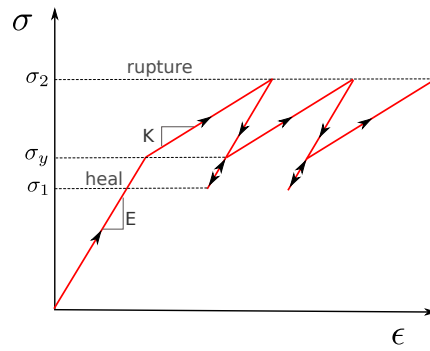


Figure S5. Schematic of the strain-stress relation for consecutive cycles for a linear elastic-plastic material with a threshold tension for rupture (σ_2) and healing (σ_1) and yield tension σ_y .

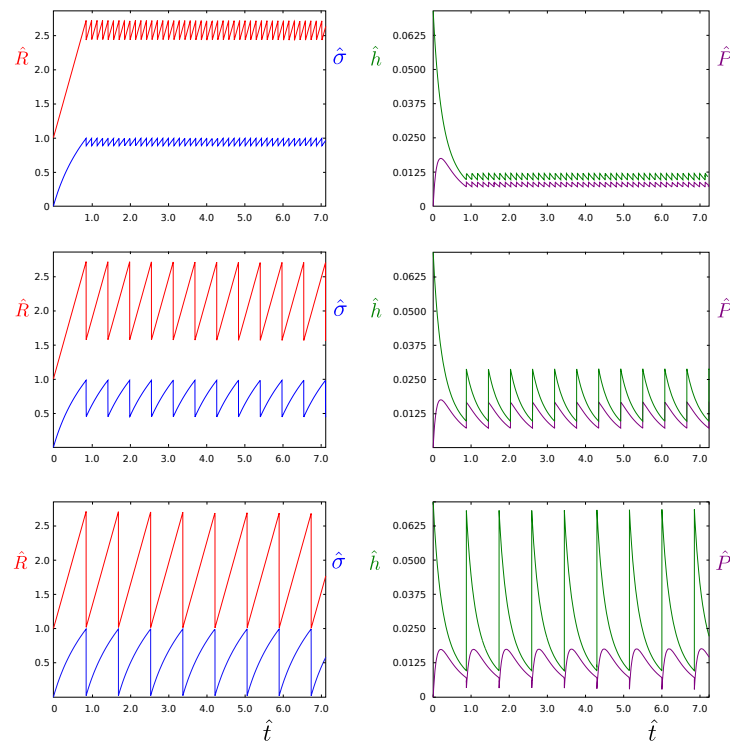


Figure S6. System dynamics for different pore closing times $\hat{\tau}_{\text{pore}} = \tau_{\text{pore}}/\tau_{\text{growth}}$. From top to bottom: $\hat{\tau}_{\text{pore}} = 5.7 \cdot 10^{-7}$, $\hat{\tau}_{\text{pore}} = 7.1 \cdot 10^{-6}$, $\hat{\tau}_{\text{pore}} = 2.9 \cdot 10^{-5}$. The rest of the dimensionless parameters are $\hat{j} = 0.008$, $e = 4.6 \cdot 10^{11}$, $\hat{\sigma}_2 = 1$, $\hat{h}_0 = 0.07$, $\hat{b}_0 = 0.036$, $\Delta\hat{\sigma} = 0.2$, $\hat{\sigma}_0 = \hat{P}_0 = 0$.

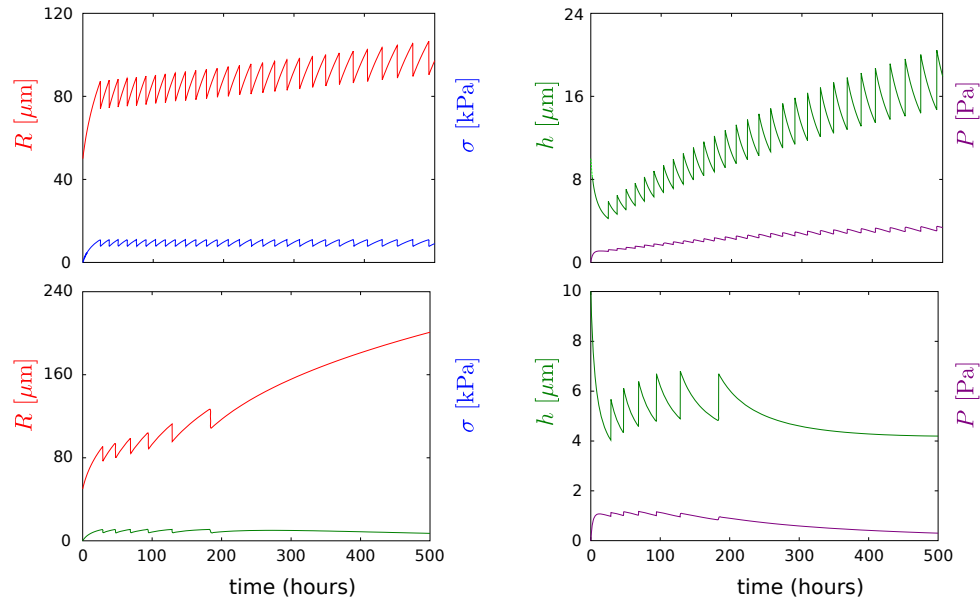


Figure S7. System trajectories for the viscoelastic case for $J_o = 25\mu\text{m}^3/\text{s}$, $J_c = 1\mu\text{m}^3/\text{s}$, $E = 20\text{kPa}$, $\sigma_2 = 11\text{kPa}$, $R_0 = 50\mu\text{m}$, $h_0 = 10\mu\text{m}$ and viscous coefficient (top) $\eta = 7.9 \cdot 10^7\text{kPa} \cdot \text{s}$ and (bottom) $\eta = 1.6 \cdot 10^7\text{kPa} \cdot \text{s}$

- [1] Alessandri, K., Sarangi, B. R., Gurchenkov, V. V., Sinha, B., Kießling, T. R., Fetler, L., Rico, F., Scheuring, S., Lamaze, C., Simon, A., Geraldo, S., Vignjevic, D., Doméjean, H., Rolland, L., Funfak, A., Bibette, J., Bremond, N., and Nassoy, P. (2013).
- [2] D. Gonzalez-Rodriguez, K. Guevorkian, S. Douezan, and F. Brochard-Wyart, “Soft matter models of developing tissues and tumors,” *Science (New York, N.Y.)*, vol. 338, pp. 910–7, Nov. 2012.
- [3] L. Preziosi, D. Ambrosi, and C. Verdier, “An elasto-visco-plastic model of cell aggregates,” *Journal of theoretical biology*, vol. 262, pp. 35–47, Jan. 2010.
- [4] J. J. Muñoz and S. Albo, “Physiology-based model of cell viscoelasticity,” *Physical Review E*, vol. 88, p. 012708, July 2013.
- [5] Koslov, M. and Markin, V. (1984). A theory of osmotic lysis of lipid vesicles. *J. Theor. Biol.*, 109(1):17–39.
- [6] Evans, E. and Heinrich, V. (2003). Dynamic strength of fluid membranes. *Comptes Rendus Phys.*, 4(2):265–274.